Research Article Vol. 33, No. 4 / 24 Feb 2025 / Optics Express 8675
Optics EXPRESS

Asymmetric point-spread function in the tilted plane

FAN WANG,[1,*] DAVID BLINDER,[1,2,3] PIN WANG,[4] YAPING ZHANG,[4] TOMOYOSHI ITO,[1] AND TOMOYOSHI SHIMOBABA[1]

[1]Graduate School of Engineering, Chiba University, 1-33 Yayoi-cho, Inage-ku, Chiba 263-8522, Japan
[2]Department of Electronics and Informatics (ETRO), Vrije Universiteit Brussel (VUB), Pleinlaan 2, Brussel 1050, Belgium
[3]IMEC, Kapeldreef 75, Leuven 3001, Belgium
[4]Yunnan Provincial Key Laboratory of Modern Information Optics, Kunming University of Science and Technology, Kunming 650500, Yunnan, China
[*]wangfan@chiba-u.jp

Abstract: In this article, we focus on the problem of sampling a point spread function (PSF) in a tilted plane for computational wave optics and holography. Conventionally, the PSF represents a symmetric wavefield distribution expressed in an orthogonal plane to the target hologram. In contrast, we reveal the wavefield for a point-spread function over a tilted plane, showing an asymmetric structure depending on the tilt angle. An asymmetric PSF formula was mathematically derived and proposed. The axial propagation of the asymmetric PSF was validated by applying it to the point-polygon hybrid method of computer-generated holograms. The off-axis propagation of the asymmetric PSF was confirmed in optical experiments by modulating the obliquely incident light with the asymmetric phase pattern uploaded to the spatial light modulator. The proposed method allows accurate off-axis light, propagation, which is not possible with a conventional symmetric PSF.

1. Introduction

Huygens' principle states that light propagates in space as a superposition of spherical waves. It posits that every point on the wavefront acts as a source of secondary spherical wavelets, which in turn propagate further. A single spherical wavefront produced by an infinitesimal point is given by the well-known point-spread function (PSF) expression [1]

$$U(r) = \frac{1}{j\lambda r}\exp(jkr), \tag{1}$$

where j is the imaginary unit, λ denotes the wavelength, $k = 2\pi/\lambda$ is the wavenumber, and r denotes the optical path length, $U(r)$ is the radially symmetric wavefront of the disturbance spreading from the source.

The PSF describes how a point source of light spreads out as a wave, while its inverse process (time reversal) can be viewed as a convergent wavefield. The PSF recorded in a plane is also known as the Fresnel zone plate, which behaves as a lens. When this PSF pattern modulates the parallel light illumination, the zone plate will refocus the light to a point. Therefore, in optical imaging, the PSF is a crucial concept for analyzing and designing optical systems, as it characterizes the response of the system to a point source input, providing a basis for determining how an optical system will image more complex objects [2,3].

The propagation of spherical waves in space is isotropic, so the wavefront recorded on a plane of a given direction will exhibit a radially symmetric structure, as shown in Fig. 1(a). The phase pattern in Fig. 1(b) describes the wavefield distribution in the plane P, given by $z = 0$, expressed

#545655 https://doi.org/10.1364/OE.545655
Journal © 2025 Received 24 Oct 2024; revised 10 Feb 2025; accepted 10 Feb 2025; published 20 Feb 2025

Optics EXPRESS

using the Cartesian coordinate system (x, y, z), which is radiated from a source point $s(x_0, y_0, z_0)$, as calculated by Eq. (1) where

$$r = \sqrt{(x - x_0)^2 + (y - y_0)^2 + z_0^2}. \tag{2}$$

Since the spatial frequency of the wavefront signal is proportional to the incidence angle, large angles may exceed the Shannon sampling limit for a regularly sampled hologram. To avoid aliasing, the wavefield is recorded in a finite region that satisfies $\sin\theta \leq \lambda/(2p)$, where θ denotes the radial angle to the propagation direction and p is the sampling pitch. For simplicity, we approximate the two-dimensional region by bounding Eq. (2) with a square-shaped pattern as shown in Fig. 1(b), which may result in undersampling at the four corners. For greater accuracy, a pincushion PSF should be used [4].

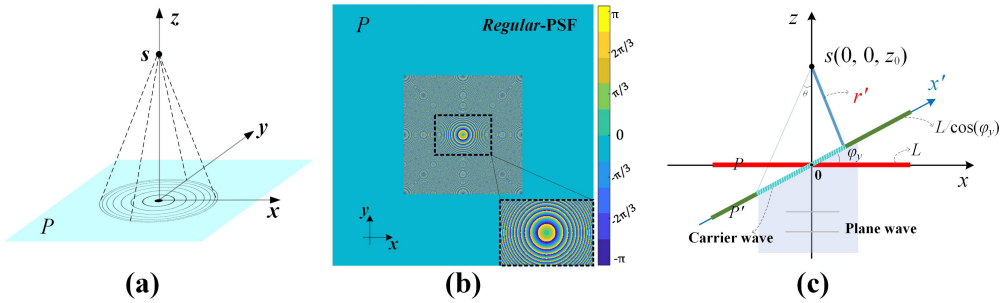

Fig. 1. (a) Schematic of a point spread wavefield to the orthogonal plane P. (b) The symmetric phase pattern on the plane P is obtained by the *regular* PSF. (c) A 2D schematic diagram: the tilted plane P' records the wavefront emitted by the source s and the plane wave propagating along the z-axis yields a carrier wave in the plane P'.

In Fig. 1(a), the recording plane is orthogonal to the propagation direction, so the phase pattern in Fig. 1(b) shows perfect symmetry, which will be referred to hereafter as *regular* PSF. However, this does not hold for the common case in which the recording plane is tilted w.r.t. the hologram plane P, as shown in the 2D profile of Fig. 1(c). A plane P' is rotated by an angle of ϕ_y around the y-axis so that it is tilted w.r.t. the plane P. The light wave emitted by the source s still propagates along the z-axis, and the wavefield is recorded in the tilted plane P'. Intuitively, the wavefield in the tilted plane P' is different from the one on the orthogonal plane P, which varies with angle and direction of inclination. In contrast to the symmetry of the *regular* PSF, the wavefield on the tilted plane may have an asymmetric structure, hence referred to as the *asymmetric* PSF (aPSF). To our knowledge, no explicit formula for mathematically describing an *asymmetric* PSF directly on the tilted plane has thus far been proposed. In this article, our objective is to mathematically derive *asymmetric* PSF, allowing the analytical calculation of the wavefield at arbitrary inclinations, which will be proposed in Section 2.

In diffraction calculations, a fundamental problem is the propagation of waves between two parallel plane segments, which is usually implemented by means of Fresnel diffraction in the spatial domain [5,6] or the angular spectrum method in the frequency domain [7,8]. The extended cases are diffraction between two parallel plane segments with a lateral offset, i.e., whose centers have different x and y coordinates; this can be solved by various variant methods of Fresnel diffraction [9] and angular spectrum diffraction [10,11]. The more general case is diffraction between two nonparallel planes, which implies a rotation of the coordinate system or a resampling of the wavefield relative to the direction of propagation. The corresponding methods for propagation along the tilted axis have also been successively derived on the basis of Fresnel diffraction [12] and angular spectrum diffraction theories [13], and interpolation

Optics EXPRESS

is often required to solve discretized coordinate grid mismatches caused by rotation [14,15]. Nonparallel propagation is essential for computer-generated holograms (CGH), especially for three-dimensional (3D) objects consisting of polygon meshes, since most of the mesh surfaces are tilted with respect to the hologram plane. In our previous work [16], we proposed treating the tilted mesh as a wavefront recording plane (WRP) and spreading the source onto the tilted WRP by the *regular* PSF. However, errors arise because the *regular* PSF expression is inaccurate for tilted planes, especially for large tilt angles. This limitation can be addressed by the *asymmetric* PSF proposed in this work, cf. Section 3.

The *regular* PSF enables on-axis focusing and is typically used for optical detection [17], imaging [18], or multi-beam laser manufacturing [19]. However, on-axis propagation in an optical setup usually requires a half-mirror to separate the incident and the reflected light, which implies a loss of the light energy. This is uneconomical for near-eye displays where power consumption is important. In contrast, the *asymmetric* PSF allows for accurate off-axis focusing of tilted incident light, which enables optical detection, off-axis imaging, or off-axis multi-beam manufacturing over a wide angular range. In the off-axis optical setup, the light energy utilization is four times of that in on-axis setup due to the saving of half-mirror. The off-axis focusing properties of the *asymmetric* PSF in the optical experiment are confirmed in Section 4.

2. Proposed method: *asymmetric* PSF

As shown in Fig. 1(c), the local coordinate system (x', y', z') of the tilted plane P' can be represent by the global coordinate system (x, y, z) as follows:

$$[x' \quad y' \quad z']^{\mathsf{T}} = \mathbf{R}[x \quad y \quad z]^{\mathsf{T}}, \tag{3}$$

where $^{\mathsf{T}}$ is the transpose operator and $\mathbf{R}$ denotes the rotation matrix, which can be derived from the normal vector of the tilted plane using Rodrigues' rotation formula to avoid the gimbal lock issue [20]. Assume that the global plane P is rotated by ϕ_x and ϕ_y around the x– and y–axes, respectively, then the rotation matrix is defined by

$$\mathbf{R} = \begin{bmatrix} r_1 & r_4 & r_7 \\ r_2 & r_5 & r_8 \\ r_3 & r_6 & r_9 \end{bmatrix}, \tag{4}$$

which is an orthogonal matrix, i.e., $\mathbf{R}^{-1} = \mathbf{R}^{\mathsf{T}}$. Therefore, Eq. (3) can be expanded to

$$\begin{cases} x = r_1 x' + r_2 y' + r_3 z' \\ y = r_4 x' + r_5 y' + r_6 z'. \\ z = r_7 x' + r_8 y' + r_9 z' \end{cases} \tag{5}$$

Since the rotation is performed around the origin point of both coordinate systems, which allows $z' = 0$ always exist, Eq. (5) can be further simplified by omitting the z' term at the end. Equation (2) gives the optical path from the source $s(x_0, y_0, z_0)$ to global coordinates, which it can be then rewritten in local coordinates based on Eqs. (2) and (5) as follows

$$r' = \sqrt{(r_1 x' + r_2 y' - x_0)^2 + (r_4 x' + r_5 y' - y_0)^2 + (r_7 x' + r_8 y' - z_0)^2}. \tag{6}$$

It is worth noting that an initial carrier wave in the tilted plane should be defined, the reason of which will be revealed by a physical property next. Generally, as shown in Fig. 1(c), a plane wave propagating in free space is defined as $\exp[j(k_x x + k_y y + k_z z)]$, where k_x, k_y and k_z represent the

Optics EXPRESS

wavenumber components on the x, y and z-axises. The case of $k_x = k_y = 0$ and $z = 0$ describes a special propagation along the z-axis and recording in the plane P, in which the wavefield is a constant. However, the tilted plane P' implies $z \neq 0$ as shown in the 2D profile of Fig. 1(c), which indicates a carrier wave written as

$$u_0 = \exp(jkz) = \exp[jk(r_7x' + r_8y')], \tag{7}$$

where $z = r_7x' + r_8y'$ is known from Eq. (5).

Based on the optical path given in Eq. (6) and the initial carrier wave given in Eq. (7), the *asymmetric* PSF to characterize the wavefield on the tilted plane P' generated by the source $s(x_0, y_0, z_0)$ is derived as

$$U'_{\text{asym}}(x', y') = u_0 \cdot \frac{1}{j\lambda r'} \exp(jkr') = \frac{1}{j\lambda r'} \exp[jk(r' + r_7x' + r_8y')], \tag{8}$$

where $U'_{\text{asym}}(x', y')$ represents the computed wavefield of the proposed *asymmetric* PSF.

Figure 2(a) shows the phase pattern of $U'_{\text{asym}}(x', y')$ distributed on the tilted plane rotated $\phi_y = 36°$ around the y-axis and $\phi_x = 45°$ around x-axis, i.e., the normal vector of the tilted plane is $\mathbf{n} = [-0.42, 0.7, 0.57]$. The rotation matrix $\mathbf{R}$ is determined by the normal vector based on Rodrigues' formula. The recording plane is sampled at a resolution of 1024×1024 with a pitch of 6.4 µm, the source point is at $(-0.8, 0.2, 25)$ mm, and the wavelength of light is defined as 633 nm. There is some unwanted aliasing noise in the wider region of the plane P' in Fig. 2(a) due to undersampling at large diffraction angles. Therefore, a quadrilateral mask is required to filter out the *asymmetric* PSF, as shown in Fig. 2(b), which corresponds to the rotation of the square region in the *regular* PSF. To obtain the quadrilateral mask, one can first geometrically solve for the four intersections of the four radial lines emanating from the source point with the tilted plane and then draw the region of interest bounded by the four points on the canvas [21].

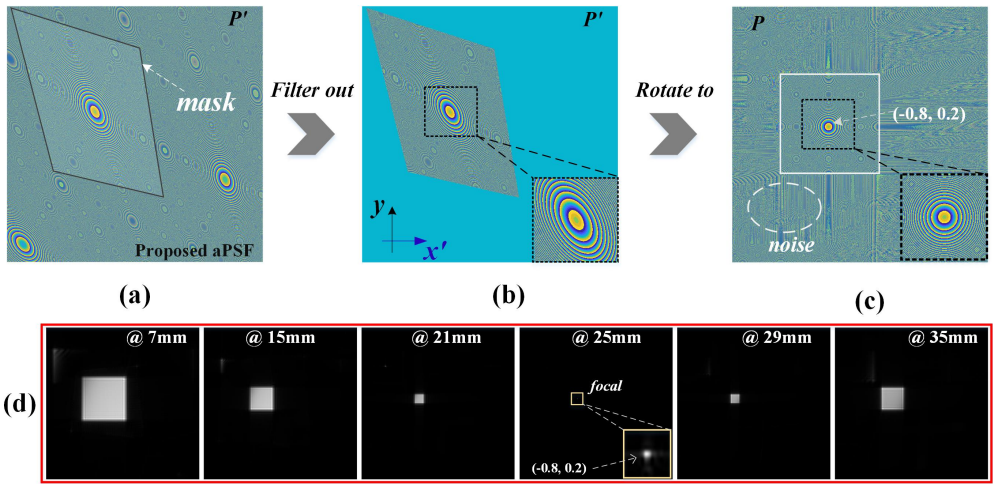

Fig. 2. (a) The phase distribution in the tilted plane P' is obtained by the proposed asymmetric PSF. (b) The phase of asymmetric PSF is filtered by the mask. (c) The phase distributed in the global plane P is obtained by rotating the phase pattern in the plane P' by spectral interpolation. (d) The rotated phase pattern of (c) is propagated to different distances, where 25 mm is the focal.

The example in Fig. 2(b) indicates that the PSF in the tilted plane is an asymmetric structure that looks like being squashed along the rotation axis. A MATLAB-based open source program for the implementation of the proposed *asymmetric* PSF can be found in Github [22].

Optics EXPRESS

To further confirm the correctness of the *asymmetric* PSF, we can obtain the wavefield in the plane P of the global system, defined as $U_{\text{glb}}(x, y)$, by rotating $U'_{\text{asym}}(x', y')$ in the frequency domain, expressed as

$$U_{\text{glb}}(x, y) = \mathfrak{Rot}_{\text{L2G}}\{U'_{\text{asym}}(x', y')\}, \tag{9}$$

where $\mathfrak{Rot}_{\text{L2G}}\{\cdot\}$ denotes the rotation operator from the local system to the global system given in Eq. (11), which is completely derived in Appendix. The phase pattern of $U_{\text{glb}}(x, y)$ is shown in Fig. 2(c), which deviates slightly from the *regular* PSF. This is because the spectral interpolation used for wavefield rotation will generate some errors, resulting in noise. However, this noise is random and weak in amplitude, so it will not affect the convergence of the wavefield. Figure 2(d) gives propagation results of $U_{\text{glb}}(x, y)$ along the z-axis at different distances, showing isotropic convergence and focusing to a point at 25 mm.

3. Axial propagation of aPSF

In CGH, the point-polygon hybrid method (PPHM) [16] leverages the PSF to first record the wavefield on the tilted polygon plane and then propagates it onto the nonparallel hologram plane using spectral interpolation of its angular spectrum, as illustrated on Fig. 3(a). This method was confirmed to yield high performance by reducing the computational effort and yielding higher visual fidelity of depth cues. However, since the PSF is supposed to be asymmetric in the tilted

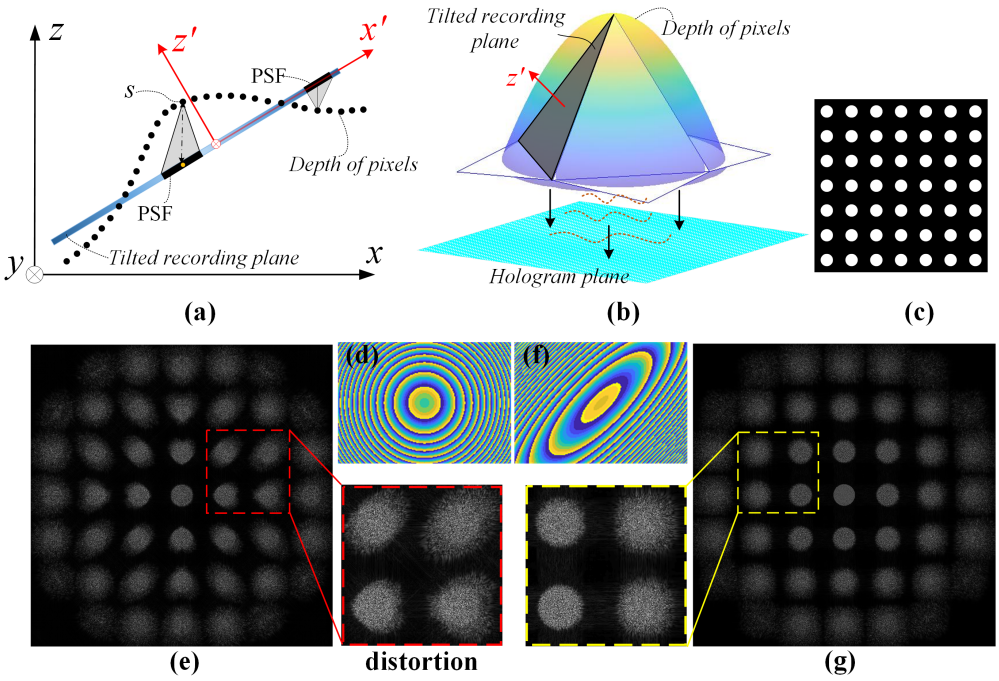

Fig. 3. (a) Schematic diagram of the PPHM [16]: the wavefront spread out from a point is recorded on the tilted plane. (b) An example of a 3D object computed using the PPHM is where the points of a smooth dome spread the wavefield over the tilted polygon surfaces. (c) The texture map used for PPHM, where the values of points on the smooth dome are extracted from. (d) is an enlargement of the *regular* PSF, and (e) is a reconstruction of a hologram generated by the *regular* PSF, showing focusing distortion. (f) is the enlargement of the proposed *asymmetric* PSF, and (g) is a reconstruction of a hologram generated by the *asymmetric* PSF, showing appropriate focus. Both (e) and (g) focus on the center of the object (Visualization 1).

Optics EXPRESS

plane, the use of the *regular* PSF will result in focusing distortion [23]. As in the example shown in Fig. 3(b), a conical polyhedron consists of four tilted triangles and four flat triangles, where the depth values of the pixels within the triangles form a dome with a smooth gradient. The intensities of pixels are given by the texture map shown in Fig. 3(c), which is a bilevel pattern consisting of small white disks on a black background.

An example of the error caused by using the *regular* PSF in this context is shown in Fig. 3(d), computing the wavefront of a single point on the tilted triangle plane. The wavefield distribution in the tilted triangle, referred to as $U'(x', y')$, is obtained by aggregating the wavefront of all pixels. The wavefield distribution in the orthogonal plane, referred to as $U_{\text{glb}}(x, y)$, is obtained by rotating $U'(x', y')$ from the local system to the global system using the rotation operator $\mathfrak{Rot}_{\text{L2G}}\{U'(x', y')\}$ given in Eq. (11). The hologram is generated by the angular spectrum method [14,16], simplified as

$$U_{\text{holo}} = \mathbf{Prop}_{\text{d}} U_{\text{glb}}(x, y), \tag{10}$$

where $\mathbf{Prop}_{\text{d}}\{\cdot\}$ denotes the propagation operator using the transfer function $H(f_x, f_y; z) = \exp\left[j2\pi f_z d\right]$, where (f_x, f_y) are the frequency coordinates in the global system, $f_z = \sqrt{\lambda^{-2} - f_x^2 - f_y^2}$ and d denote the propagation distance. The inverse process of propagation of the angular spectrum for U_{holo} can bring the pattern back in focus, as shown in Fig. 3(e) focusing on the topmost part of the dome, i.e., the center circle of the texture map. Obviously, the defocused area shows an asymmetric diffusion in Fig. 3(e), as if being squashed, which is highlighted by the enlarged portion. This distortion indicates that the *regular* PSF does not accurately represent the wavefield distribution in the tilted plane.

Instead, we argue that an *asymmetric* PSF should be used to characterize the wavefield distribution in the tilted plane. As derived in Section 2, we can obtain the transform matrix by the normal of the tilted plane in Fig. 3(b), and then compute the wavefront of a point by the proposed Eq. (8), the partial enlargement of which is shown in Fig. 3(f). The hologram is generated by performing Eq. (10), and the same focal reconstruction is shown in Fig. 3(g), presenting the expected symmetric diffusion, which differs from the squashed diffusion for Fig. 3(e). Visualization 1 gives reconstructed animations of the focus changes in Figs. 3(e) and (g).

The above example demonstrates that the proposed *asymmetric* PSF can accurately describe the wavefront of the PSF in the tilted plane. Utilizing it in the PPHM for CGH confirms the feasibility of the *asymmetric* PSF for axial propagation.

4. Off-axis propagation of aPSF

Typically, a PSF acts like a lens that converges incoming parallel light to a focal point along the propagation axis, but only if it is a *regular* PSF and the incoming light is incident orthogonally. Figure 4(a) shows the optical setup for orthogonal incidence, where a half mirror must be used to separate the input and output paths, implying that only 25% of the light can be utilized. It is well-known that liquid crystal-based spatial light modulators (SLMs) can modulate the phase of incoming light. A phase-only SLM with a pixel pitch of 3.74 µm with a resolution of 3840×2160 is used to modulate the incident light and the camera is for detecting modulated light. The camera can be shifted along the reflection axis of the SLM panel. Figure 4(c) shows the calculated phase pattern for the *regular* PSF consisting of a sequence of 5×3 points, each increasing in depth by 5 mm from top to bottom and left to right. The first point (top left) is placed at a distance of 20 cm, and the last point (bottom right) is at 27 cm. Figure 5(a) shows the detection results for the reference case using the *regular* PSF of Fig. 4(c) in an on-axis optical setup shown on Fig. 4(a). The four pictures in Fig. 5(a) are focused on different positions, respectively, presenting isotropic convergence and converging into a sharp dot at the focused location. Visualization 2 provides an animation of the camera moving along the axis.

Optics EXPRESS

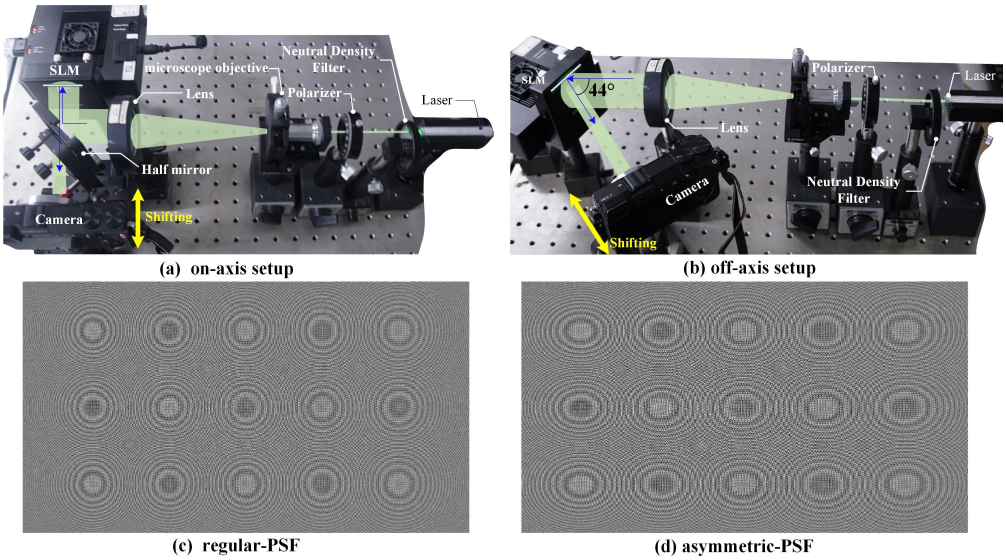

Fig. 4. (a) On-axis optical setup for orthogonal incidence onto the SLM. (b) Off-axis optical setup for slanted incidence onto the SLM. (c) The phase pattern of the *regular* PSF consists of an array of 5×3 dots. (d) The phase pattern of the *asymmetric* PSF with a y-axis tilted angle 22°.

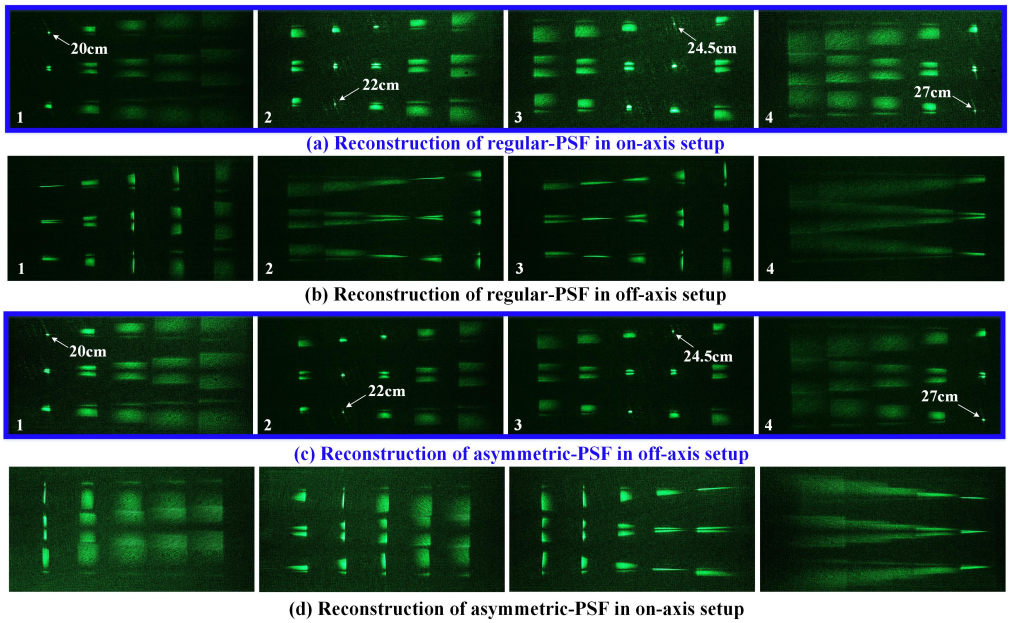

Fig. 5. Reconstructed images at different positions modulated by SLM. (a) The regular PSF phase pattern is modulated by orthogonal incidence in Fig. 4(a). (b) The regular PSF phase pattern is modulated by slanted incidence. (c) The proposed asymmetric PSF phase pattern is modulated by slanted incidence. (d) The proposed asymmetric PSF phase pattern is modulated by orthogonal incidence in Fig. 4(a). The animations of a shifting camera see in Visualization 2.

Optics EXPRESS

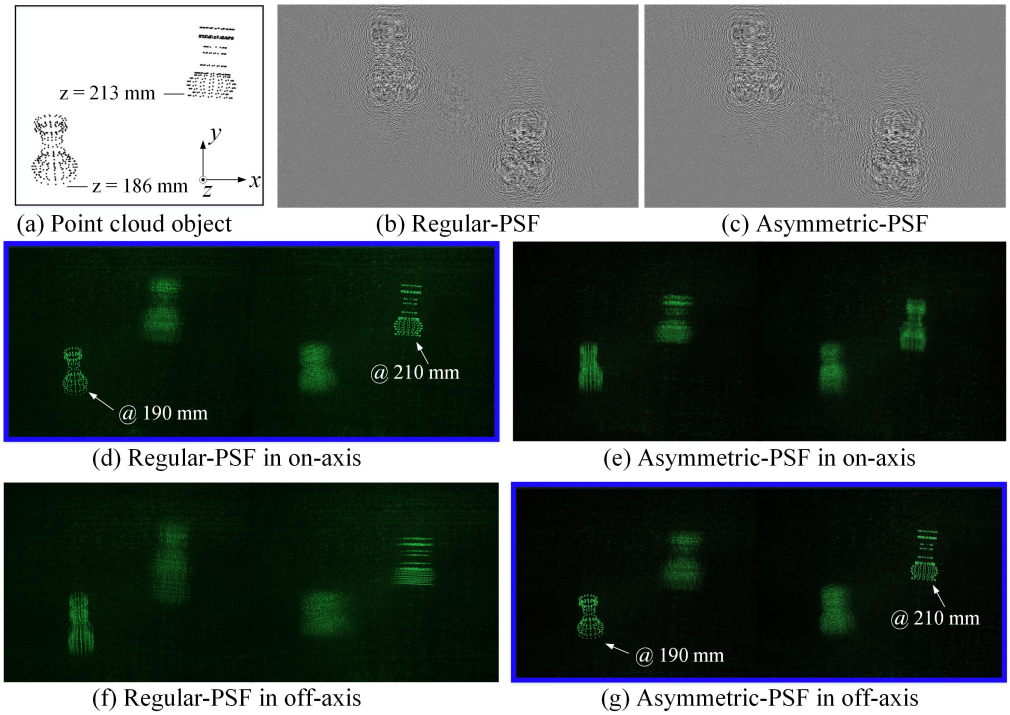

Fig. 6. (a) 3D point cloud model of chess pieces. (b) The hologram generated by the *regular* PSF. (c) The hologram generated by the *asymmetric* PSF. (d) Reconstructions of the *regular* PSF hologram and (e) reconstructions of the *asymmetric* PSF in the on-axis setup. (f) Reconstructions of the *regular* PSF hologram and (f) reconstructions of the *asymmetric* PSF in the off-axis setup. See the corresponding animations in Visualization 3.

Conversely, if light is incident at an angle on the SLM while using a *regular* PSF phase pattern, as shown in Fig. 4(b), where the incident angle is approximately 22°, the modulated light in the reflected direction will lose its isotropic focusing property. This is demonstrated in Fig. 5(b), where the focal locations converge into a line instead of a point because the divergence along the y-axis does not harmonize with the divergence along the x-axis; see Visualization 2. It is worth noting that no half mirror is required for oblique incidence, which means that the light energy utilization is four times higher compared to the on-axis setup where a half mirror is required.

As discussed in Section 2, in the case of oblique incidence, one should utilize the asymmetric PSF phase pattern, as expressed in Eq. (8) according to the tilt angle, given in Fig. 4(d). Figure 5(c) shows the reconstructed results of using the *asymmetric* PSF of Fig. 4(d) in the off-axis optical setup of Fig. 4(b). The modulated light along the off-axis direction for the asymmetric PSF phase exhibits the same isotropy as the regular PSF phase of orthogonal incidence in Fig. 5(a), the in-focus position converges to a point, while the out-of-focus position diverges anisotropically; see Visualization 2. As a comparison, the *asymmetric* PSF phase pattern is also used to modulate the orthogonal incident light, and the results are shown in Fig. 5(d) with the same anisotropy as that in Fig. 5(b); see Visualization 2.

To further validate the *asymmetric* PSF, two chess pieces consisting of 564 points, shown in Fig. 6(a), are used to generate holograms by aggregating all the point-spread functions. The center of the two pieces are located at 186 mm and 213 mm, respectively. The holograms computed by the *regular* PSF and by the *asymmetric* PSF are shown in Fig. 6(b) and Fig. 6(c), respectively. The parameters of holograms are consistent with those of the SLM. Figure 6(d) shows results of

Optics EXPRESS

the *regular* PSF hologram reconstructed in an on-axis optical setup (cf. Figure 4(a)), where the front piece and the rear piece are focused, respectively. However, the reconstructions of *regular* PSF hologram by the off-axis optical setup show focusing distortion, as shown in Fig. 6(e). The same distortion also occurs in the reconstructions of the *asymmetric* PSF hologram in the on-axis optical setup, as shown in Fig. 6(f). The appropriate way is to reconstruct the *asymmetric* PSF hologram in the off-axis optical setup, as shown Fig. 6(g), with the same focusing distance and convergence image as in Fig. 6(d). The corresponding animations created by a moving camera can be seen in Visualization 3.

From the results of the experiments shown in Figs. 5 and 6, it can be confirmed that the *regular* PSF will match only the orthogonal incident light, whereas the *asymmetric* PSF will match incident light at a tilted angle. This difference gets more pronounced as the tilt angle increases.

5. Conclusion

The point-spread function describes a regular wavefield distribution in an orthogonal plane that exhibits rotational symmetry. However, the spread wavefield in a tilted plane was confirmed as an asymmetric structure, where the asymmetry arises from the nonlinear stretching of the sampling coordinates. This article revealed this physical mechanism in Section 2 and rigorously derived the *asymmetric* PSF formula as Eq. (8), showing that the asymmetric wavefield distribution depends on the tilted angle.

In the case where the tilted plane is used as the WRP, all points diffuse the light wave towards the tilted polygonal surface, which should be done by the *asymmetric* PSF. Based on the results of axial propagation without distortion of the tilted plane, the *asymmetric* PSF effectively corrects the inaccuracies in PPHM [16] that arise when using the *regular* PSF to record the wavefield of tilted polygonal surfaces.

The zone plate generated by the *regular* PSF can only converge orthogonal incident light to a focal point, implying distortion or anisotropic convergence for off-axis incidence. The optical experiment with off-axis incidence using the asymmetric PSF phase pattern verified isotropic convergence at arbitrary tilted angles, enabling optical imaging at larger fields of view and saving up to three times the illumination power for the display system.

The proposed *asymmetric* PSF formula complements the *regular* PSF, making the propagation and recording of light waves more universally applicable in mathematical descriptions.

Appendix: Spectral rotation from the local system to the global system

This appendix elaborates on how to obtain the wavefield distribution of the global system (x, y, z) from the known wavefield of the local system (x', y', z'), i.e., rotating the spectrum of the local system to the global system. Suppose the known wavefield in the $z' = 0$ plane of the local system as $U'(x', y', z' = 0)$, which also can be represented in the global coordinates as $U(x, y, z \neq 0)$. Then, the wavefield distributed on the z=0 plane of the global system, $U(x, y, z = 0)$, can be obtained by the operator

$$U(x, y, z = 0) = \mathfrak{Rot}_{\mathrm{L2G}}\{U'(x', y', z' = 0)\}, \tag{11}$$

which is derived as follows.

By Fourier transform, the spectrum of $U(x, y, z)$ in the global system can be expressed as

$$A(f_x, f_y) = \iint U(x, y, z) \cdot e^{-j2\pi(f_x x + f_y y + f_z z)} \mathrm{d}x\mathrm{d}y. \tag{12}$$

Due to the rotational transform of the matrix $\mathbf{R}$, the integral expression above undergoes a coordinate transform, rewritten as

$$A(f_x, f_y) = J \iint U'(x', y', z') e^{-j2\pi(\hat{f}_x x' + \hat{f}_y y')} \mathrm{d}x'\mathrm{d}y', \tag{13}$$

Optics EXPRESS

where $J = |r_1 r_5 - r_2 r_4|$ is the Jacobian determinant, and

$$\begin{cases} \hat{f}_x = r_1 f_x + r_4 f_y + r_7 (f_z - 1/\lambda) \\ \hat{f}_y = r_2 f_x + r_5 f_y + r_8 (f_z - 1/\lambda). \end{cases} \tag{14}$$

The new frequency coordinates $(\hat{f}_x, \hat{f}_y)$ are not sampled with equal spacing, making it impossible to calculate the integral term in Eq. (13) using the Fast Fourier Transform (FFT) in numerical calculations. Therefore, an interpolation operation is suggested to calculate Eq. (13) as follows:

$$\mathbf{A}(f_x, f_y) = J\Theta_{(f'_x, f'_y)}^{(\hat{f}_x, \hat{f}_y)} \mathcal{F}[U'(x', y')], \tag{15}$$

where $\mathcal{F}[U'(x', y')]$ denotes the FFT operation based on the equally spaced sampling grid (f'_x, f'_y), and $\Theta_{(f'_x, f'_y)}^{(\hat{f}_x, \hat{f}_y)}$ denotes the interpolation of the sampling grid $(\hat{f}_x, \hat{f}_y)$ into the sampling grid (f'_x, f'_y) to obtain the spectrum under the sampling coordinates $(\hat{f}_x, \hat{f}_y)$.

Finally, the wavefield distributed on the $z = 0$ plane of the global system can be computed as

$$U(x, y, z = 0) = \mathcal{F}^{-1}[A(f_x, f_y)] = J \cdot \mathcal{F}^{-1} \left\{ \Theta_{(f'_x, f'_y)}^{(\hat{f}_x, \hat{f}_y)} \mathcal{F}[U'(x', y')] \right\}, \tag{16}$$

where $\mathcal{F}^{-1}$ denotes the inverse FFT. This corresponds to the rotation operator defined in Eq. (11).

Funding. Japan Society for the Promotion of Science (P22752, P23378, 22H03607); Institute for Global Prominent Research, Chiba University; National Natural Science Foundation of China (62275113); Fonds Wetenschappelijk Onderzoek (G089424N, G0A3O24N).

Acknowledgements. We thank Prof. Hao Zhang of Tsinghua University, China, for his early discussions.

Disclosures. The authors declare no conflicts of interest.

Data availability. The MATLAB code generated during the current study are available in the Github repository [22].

References

1. J. W. Goodman, *Introduction to Fourier optics* (Roberts and Company publishers, 2005).
2. J. J. Braat, S. van Haver, A. J. Janssen, *et al.*, "Assessment of optical systems by means of point-spread functions," Prog. Opt. **51**, 349–468 (2008).
3. Z. Tian, L. Li, J. Ma, *et al.*, "Cfza camera: a high-resolution lensless imaging technique based on compound fresnel zone aperture," Opt. Lett. **49**(12), 3532–3535 (2024).
4. D. Blinder, T. Birnbaum, and P. Schelkens, "Pincushion point-spread function for computer-generated holography," Opt. Lett. **47**(8), 2077–2080 (2022).
5. D. G. Voelz and M. C. Roggemann, "Digital simulation of scalar optical diffraction: revisiting chirp function sampling criteria and consequences," Appl. Opt. **48**(32), 6132–6142 (2009).
6. S. Fujimori, T. Ito, and T. Shimobaba, "Further aliasing-reduced shifted and scaled fresnel diffraction," Opt. Lasers Eng. **173**, 107918 (2024).
7. K. Matsushima and T. Shimobaba, "Band-limited angular spectrum method for numerical simulation of free-space propagation in far and near fields," Opt. Express **17**(22), 19662–19673 (2009).
8. F. Wang, T. Shimobaba, T. Kakue, *et al.*, "Controllable energy angular spectrum method," Opt. Commun. **520**, 128506 (2022).
9. R. P. Muffoletto, J. M. Tyler, and J. E. Tohline, "Shifted fresnel diffraction for computational holography," Opt. Express **15**(9), 5631–5640 (2007).
10. K. Matsushima, "Shifted angular spectrum method for off-axis numerical propagation," Opt. Express **18**(17), 18453–18463 (2010).
11. H.-h. Son and K. Oh, "Light propagation analysis using a translated plane angular spectrum method with the oblique plane wave incidence," J. Opt. Soc. Am. A **32**(5), 949–954 (2015).
12. K. Yamamoto, Y. Ichihashi, T. Senoh, *et al.*, "Calculating the fresnel diffraction of light from a shifted and tilted plane," Opt. Express **20**(12), 12949–12958 (2012).
13. N. Delen and B. Hooker, "Free-space beam propagation between arbitrarily oriented planes based on full diffraction theory: a fast fourier transform approach," J. Opt. Soc. Am. A **15**(4), 857–867 (1998).
14. K. Matsushima, H. Schimmel, and F. Wyrowski, "Fast calculation method for optical diffraction on tilted planes by use of the angular spectrum of plane waves," J. Opt. Soc. Am. A **20**(9), 1755–1762 (2003).

Optics EXPRESS

15. S. J. Jeong and C. K. Hong, "Pixel-size-maintained image reconstruction of digital holograms on arbitrarily tilted planes by the angular spectrum method," Appl. Opt. **47**(16), 3064–3071 (2008).
16. F. Wang, D. Blinder, T. Ito, *et al.*, "Point-polygon hybrid method for generating holograms," Opt. Lett. **48**(12), 3339–3342 (2023).
17. C. Hao, S. Gao, Q. Ruan, *et al.*, "Single-layer aberration-compensated flat lens for robust wide-angle imaging," Laser Photonics Rev. **14**(6), 2000017 (2020).
18. F. Liu, J. Wu, and L. Cao, "Autofocusing of fresnel zone aperture lensless imaging for qr code recognition," Opt. Express **31**(10), 15889–15903 (2023).
19. W. Ge, C. Xing, V. Veiko, *et al.*, "All-optical, self-focused laser beam array for parallel laser surface processing," Opt. Express **27**(20), 29261–29272 (2019).
20. E. Pi na, "Rotations with rodrigues' vector," Eur. J. Phys. **32**(5), 1171–1178 (2011).
21. K.-h. Park and H. W. Park, "Region-of-interest coding based on set partitioning in hierarchical trees," IEEE Trans. Circuits Syst. Video Technol. **12**(2), 106–113 (2002).
22. Github, Asymmetric-psf, 1.0, Github, (2024).https://github.com/phywangfan/asymmetric-PSF.git
23. D. Arai, T. Shimobaba, K. Murano, *et al.*, "Acceleration of computer-generated holograms using tilted wavefront recording plane method," Opt. Express **23**(2), 1740–1747 (2015).